J. Fluid Mech. (1966), *vol.* 25, *part* 1, *pp.* 185–198
Printed in Great Britain

The shape of low-speed capillary jets of Newtonian liquids

By SIMON L. GOREN AND STANISLAW WRONSKI†
Department of Chemical Engineering, University of California, Berkeley, California

(Received 30 August 1965)

The shape of a jet of Newtonian liquid issuing from a capillary needle into air is considered. The results of two theoretical approaches are presented. One approach is a perturbation analysis about the final state of the jet and the other is a boundary-layer analysis near the point of jet formation. Comparison of the predictions with experimental jet shapes shows them to be in semi-quantitative agreement. Especially interesting is the presence of a 'discontinuity' in the empirical exponential decay rate of the jet radius occurring at a Reynolds number somewhere between 14 and 20 and the correspondence of this discontinuity with the peculiar behaviour in this range of the Reynolds number of the theoretical eigenvalue.

1. Introduction

The liquid in a laminar jet issuing from a long capillary needle into an immiscible and inviscid medium (such as air) experiences a sudden elimination of the viscous shear stress at the newly formed jet surface. In the absence of gravitational effects, the removal of this shear stress results in the relaxation of the velocity profile until plug flow is established at some distance sufficiently far from the needle exit. Accompanying the velocity rearrangement is a change in jet diameter. Neglecting viscous forces, Harmon (1955) made mass and momentum balances for the jet between the exit, where the velocity profile is taken to be parabolic, and a point far downstream where the velocity profile has become flat. This straightforward calculation leads to the result that the average velocity increases to $\frac{4}{3}$ times the initial average velocity, $\overline{w}_0$, and the jet diameter therefore decreases to $\sqrt{(3)}/2\,(=0{\cdot}866)$ times the initial jet diameter, $2a_0$. If viscous forces are present in the jet, and indeed they must be to effect the profile rearrangement, then the final velocity will be less than $\frac{4}{3}\,\overline{w}_0$ because some of the kinetic energy of the jet will be dissipated into heat. Consequently the final jet radius will not be decreased as greatly as suggested by Harmon. In fact, under certain conditions the viscous dissipation is so great that the jet actually slows down and its diameter increases. This problem has been discussed by Middleman & Gavis (1961) and Gavis (1964). They present a correlation for the ratio, χ, of the final jet diameter to the initial jet diameter as a function of the Reynolds number, $2a_0\overline{w}_0/\nu$, based on the initial jet diameter and the initial average velocity. For

† Now at Warsaw Technical University, Warsaw, Poland.

the Reynolds numbers less than about 16 the jets expand; for the Reynolds numbers greater than 16 they contract. As the Reynolds number becomes large, χ seems to approach the value predicted by Harmon. In a later paper Middleman (1964) used a von Kármán-type integral approach in an attempt to calculate the velocity profile and jet diameter as functions of the distance from the needle exit. His calculation is limited to the high Reynolds numbers since χ was taken to be $\sqrt{(3)}/2$. Furthermore, as Middleman points out, the results are dependent upon his choice of a matching condition which essentially fixes the location of the theoretical curve in his figure 2.

There are two papers dealing with an almost identical problem, namely, finding the length required to attain plug flow in a jet issuing from an orifice where the initial velocity profile is flat except for a very thin peripheral layer through which the velocity drops to zero. Bohr (1909), in seeking an order-of-magnitude estimate for this length, made certain approximations in the equations of motion and sought solutions decaying exponentially in axial distance. It turns out that Bohr's theory is applicable to the present problem at 'large' distances from the needle exit but, because of the approximations he made, its validity is limited to the large Reynolds numbers (greater than about 40). For the same problem (but with the added complication of gravitational acceleration in a vertically-oriented jet) Scriven & Pigford (1959) used the boundary-layer theory previously developed by Goldstein (1930) for an analogous problem to predict the surface velocity as a function of the distance from the exit. They found that the surface velocity initially increases as the cube root of the axial distance.

In this paper we shall discuss the results of two theoretical approaches which enable us to predict certain characteristics of the jet shape. One approach, valid for large axial distances, is a perturbation analysis about the final state of the jet. It leads to an interesting eigenvalue problem, which for the large Reynolds numbers reduces to the problem already investigated by Bohr. For the low Reynolds number (< 16) the eigenvalues show an unexpectedly peculiar behaviour which is somewhat reproduced in the experimental data. The second approach is a boundary-layer treatment valid for short axial distances and the large Reynolds numbers which predicts that the surface velocity and change in jet radius both increase as the cube root of the axial distance. In the treatment it is necessary to take into account explicitly the (spatially) changing surface in order that the coefficients of the cube root may be calculated.

The following notation is used:

a jet radius;
g velocity function for boundary-layer analysis;
p pressure;
r radial co-ordinate;
Re $= 2aw/\nu$, the Reynolds number;
S $= \rho\sigma a/\mu^2$, surface-tension parameter;
u radial velocity;
w axial velocity;
y distance from free surface;
z axial co-ordinate;

β a constant;
γ eigenvalue;
ζ $= (a_0 - a)$, deviation of jet surface from $r = a_0$;
η $= (4\bar{w}_0 y^3/3a_0\nu z)^{\frac{1}{3}}$, similarity variable;
μ viscosity;
ν kinematic viscosity;
ρ density;
σ surface tension;
χ $= a_\infty/a_0$, ratio of final jet diameter to initial jet diameter;
ψ stream function;
0 subscript denoting value at needle exit;
∞ subscript denoting value at final jet state;
$\hat{}$ superscript denoting perturbation from value at final jet state;
$\bar{}$ superscript denoting average across jet cross-section.

2. Theory

We shall consider the jet to be composed of a Newtonian liquid of constant physical properties. The only surface property of importance is the surface tension. It is assumed that the jets are formed and remain axially symmetric, and are not affected by gravity or the surrounding medium. (This actually restricts the velocity to a range, low enough that air friction is unimportant and yet high enough that the profile relaxation is complete before the jet has been accelerated by gravity.) Infinitely far from the needle exit the jet will approach its final state of radius a_∞, axial velocity w_∞, pressure $p_\infty = \sigma/a_\infty$ and zero radial velocity. Very far from the needle exit, the velocity, jet radius and pressure will be slightly different from these final values. Thus we put

$$\left.\begin{aligned} w &= w_\infty + \hat{w} = w_\infty - \frac{1}{r}\frac{\partial\hat{\psi}}{\partial r}, \\ u &= 0 + \hat{u} = \frac{1}{r}\frac{\partial\hat{\psi}}{\partial z}, \\ p &= p_\infty + \hat{p}, \quad a = a_\infty + \hat{a}, \end{aligned}\right\} \tag{1}$$

where the perturbations (represented by $\hat{}$) are considered to be so small that second-order terms in them may be neglected in the ensuing theory. In the above we also introduce the perturbation stream function which identically satisfies the continuity equation because of the axial symmetry. When these expressions are substituted into the Navier–Stokes equations and only the linear terms are retained and when the pressure is eliminated between the two equations the following equation for the disturbance stream function is obtained:

$$\left.\begin{aligned} &\mathscr{D}\left(\mathscr{D} - \frac{w_\infty}{\nu}\frac{\partial}{\partial z}\right)\hat{\psi} = 0, \\ \text{where} \quad &\mathscr{D} \equiv \frac{\partial^2}{\partial r^2} - \frac{1}{r}\frac{\partial}{\partial r} + \frac{\partial^2}{\partial z^2}. \end{aligned}\right\} \tag{2}$$

The solution to this differential can be expressed in the form

$$\hat{\psi} = \left\{A\frac{\gamma r}{a_\infty}J_1(\gamma r/a_\infty) + B\frac{\gamma r}{a_\infty}Y_1(\gamma r/a_\infty) + C\frac{\gamma^* r}{a_\infty}J_1(\gamma^* r/a_\infty) + D\frac{\gamma^* r}{a_\infty}Y_1(\gamma^* r/a_\infty)\right\} e^{-\gamma z/a_\infty}, \tag{3}$$

where $\gamma^{*2} = \gamma^2 + \frac{1}{2}\gamma\, Re_\infty$,

and $Re_\infty = 2a_\infty w_\infty/\nu$.

The final Reynolds number, Re_∞, is related to the Reynolds number based on the initial jet diameter and the initial average velocity by $Re_\infty = Re/\chi$ and since χ changes by about 15% at most, the two Reynolds numbers have roughly equivalent numerical values. $J_n(x)$ and $Y_n(x)$ are Bessel functions of order n, and A, B, C, D, are constants to be determined by the boundary conditions.

The conditions that the radial velocity vanishes and the axial velocity remains finite at the jet centre require that the constants B and D be zero. At the free surface the tangential shear stress is zero and the change in normal stress across the free surface is due to the latter's curvature and the interfacial surface tension. In addition, the location of the free surface is given by the kinematic condition $u_{\text{surface}} = Da/Dt$ (or alternately by the condition of constant volumetric flow-rate). To the order of approximation considered here, these conditions may be written in terms of the disturbance stream function as

$$\hat{a} = (1/a_\infty w_\infty)\,\hat{\psi}(a_\infty, z), \tag{4}$$

and

$$\left\{\mathscr{D} - 2\frac{\partial^2}{\partial z^2}\right\}\hat{\psi} = 0, \tag{5}$$

$$\int_\infty^z \frac{1}{r}\frac{\partial}{\partial r}\left\{\mathscr{D} - \frac{w_\infty}{\nu}\frac{\partial}{\partial z}\right\}\hat{\psi}\,dz + 2\frac{\partial}{\partial r}\frac{1}{r}\frac{\partial\hat{\psi}}{\partial z} = \frac{\sigma}{\mu a_\infty^3 w_\infty}\left\{\hat{\psi} + a_\infty^2\frac{\partial^2\hat{\psi}}{\partial z^2}\right\} \tag{6}$$

at $r = a_\infty$. When the stream function given by (3) is substituted into (5) and (6) two linear, homogeneous equations for the constants A and B are obtained. A non-trivial solution exists only if the determinant of the coefficients vanishes. This leads to the following eigenvalue equation for determining the damping factor, γ:

$$4\gamma^4\{\gamma^* J_0(\gamma^*)/J_1(\gamma^*)\} + (\gamma^{*2} - \gamma^2)\,2\gamma^2 - (\gamma^{*2} + \gamma^2)^2\{\gamma J_0(\gamma)/J_1(\gamma)\} = S(1+\gamma^2)\,\gamma^2, \tag{7}$$

in which the group $S = \rho\sigma a_\infty/\mu^2$ has been chosen to characterize the role of the surface tension instead of the Weber number because this group is independent of the jet velocity. Thus γ can be determined as a function of Re_∞ and S. Actually, (7) permits an infinite number of solutions, so that the perturbations would be expressed as infinite series, the coefficients in these series to be found by an appropriate weighting technique. If one gets sufficiently far from the needle exit, only the term with the lowest eigenvalue should be important since its decay rate is the slowest.

We have calculated the lowest eigenvalue. The determination of the eigenvalues from (7) by trial and error is an easy calculation for the large final Reynolds numbers. The values obtained are independent of the surface-tension parameter S. As the final Reynolds number tends towards infinity the eigenvalue is given by the relation $\gamma = 29{\cdot}36/Re_\infty$, which is the result obtained by Bohr by neglecting the second derivative with respect to axial distance in the Laplacian operator. Below a final Reynolds number of about 40 the eigenvalues deviate from Bohr's values and the surface-tension group becomes an important parameter. For the

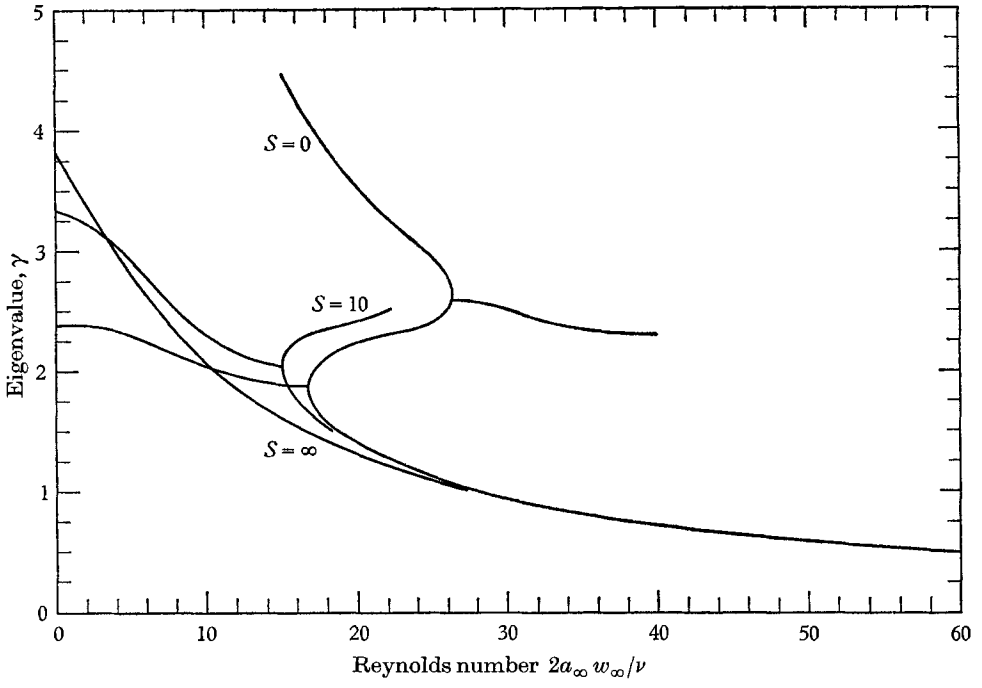

FIGURE 1. The lowest eigenvalue as a function of the final Reynolds number, $2a_\infty w_\infty/\nu$, and the surface tension parameter, $\rho\sigma a_\infty/\mu^2$. *Note*: where the eigenvalue is complex only the real part is shown.

typical case $S = 0$, as the Reynolds number is decreased below 40 the γ *vs.* Re_∞ curve becomes steeper and steeper until it obtains an infinite slope at $Re_\infty = 16{\cdot}8$, $\gamma = 1{\cdot}86$. The curve then smoothly doubles back on itself, i.e. γ increasing with Re_∞ increasing, until a second point of infinite slope is reached at $Re_\infty = 26{\cdot}6$, $\gamma = 2{\cdot}65$ (see figure 1). The curve then doubles back on itself a second time, with γ now increasing as Re_∞ decreases. This reversal is repeated over and over again until the curve becomes asymptotic to the line $Re_\infty = 4\pi$. For certain values of the final Reynolds number, (7) permits complex eigenvalues. In fact each point of infinite slope of the γ *vs.* Re_∞ curve is a bifurcation point from which two complex (conjugate) solutions spring. These complex eigenvalues were determined by a trial and error procedure using a digital computer. The results of the calculations are shown in figure 1; in regions where the eigenvalue is complex only the real part is shown. Analogous curves exist for other values

of the surface-tension group except that when $S = \infty$ the eigenvalue is a real, single-valued function of the Reynolds number over the entire Reynolds-number range.

Thus, this approach predicts that sufficiently far from the needle exit the jet radius and velocities decay exponentially to their final values. The eigenvalue problem gives the rate of decay as a function of the final Reynolds number and the surface-tension group. (In regions were the eigenvalue is multi-valued some difficulty in choice arises.) However, the magnitude of the deviation from the final state cannot be calculated until the initial conditions at the needle exit are imposed. This is complicated by the fact that the equation for the stream function is a fourth-order equation rather than belonging to the well-investigated second-order Sturm–Liouville system. Even so, the assumption that the flow is only slightly perturbed from the final state is not valid near the needle exit. One is therefore forced to seek a solution which is valid near the needle exit and to try to match this with the above perturbation solution. As a first approximation to a solution which is valid near the needle exit, we have examined the boundary-layer problem sketched below. The details of this analysis will be presented elsewhere.

The defining property of this flow is the instantaneous removal of the wall shear stress at the needle exit. At the high Reynolds numbers, at least, the shear stress in the fluid must therefore fall from some finite value at a point slightly within the jet to zero at the jet surface; i.e. there is a peripheral boundary layer in which the removal of the large wall shear stress is felt. It is plausible that near the needle exit the interaction of the peripheral region of the jet with the faster moving core is negligible. (An attempt to take this interaction into account was made, but the calculation then becomes immensely more complicated.) Near the jet surface the Poiseuille parabolic velocity profile can be approximated as $w = (4\bar{w}_0/a_0)(\zeta + y)$, where y is the distance into the liquid from the free surface and ζ is the deviation of the jet surface from $r = a_0$. Assuming a flow which deviates from the above only near $y = 0$ one may apply the standard (two-dimensional) boundary-layer equations to calculate the velocity profile and change in jet radius. Fortunately, the problem admits a similarity solution. With the velocity given as

$$w = (4\bar{w}_0/a_0)\{\zeta(z) + y + (3\nu z a_0/4\bar{w}_0)^{\frac{1}{3}} g(\eta)\}, \tag{8}$$

where

$$\eta = (4\bar{w}_0 y^3/3a_0\nu z)^{\frac{1}{3}},$$

the following ordinary equation for $g(\eta)$ is obtained:

$$g'' = (\beta + \eta + g)(\beta + g - \eta g') - \left(\beta\eta + 2\int_0^\eta g\,d\eta - \eta g\right)(1 + g'). \tag{9}$$

The boundary conditions for zero shear stress at the free surface and for the vanishing of the modification of the velocity far from the free surface are

$$\left.\begin{aligned} &\text{at} \quad \eta = 0, \quad g' = -1, \\ \text{and} \quad &\text{at} \quad \eta = \infty, \quad g = 0. \end{aligned}\right\} \tag{10}$$

In addition, the constraint of constant volumetric flow rate must be satisfied and this imposes the following condition which determines the constant β:

$$\beta^2 = 2\int_0^\infty g\,d\eta. \tag{11}$$

The problem was solved by the method of Meksyn (1961), namely by seeking a power-series solution for small η, and then applying the boundary condition at infinity in terms of an integral which is evaluated by the method of steepest descents. The result is similar to that of Scriven & Pigford in that both the surface velocity and the change in jet radius increase as the cube root of the axial distance. They are given by the following formulae:

$$\left.\begin{aligned} \zeta/a_0 &= (a_0 - a)/a_0 = 0{\cdot}703\,\{(z/a_0)/(2a_0\bar{w}_0/\nu)\}^{\frac{1}{3}}, \\ w_{\text{surf}}/\bar{w}_0 &= 5{\cdot}07\,\{(z/a_0)/(2a_0\bar{w}_0/\nu)\}^{\frac{1}{3}}. \end{aligned}\right\} \tag{12}$$

It is interesting to note that, for the large Reynolds numbers, both approaches give the jet shape as a function of the group z/aRe.

3. Experiment

The jets were produced by forcing liquid from a reservoir through capillary nozzles. Three liquids: white oil, a glycerol–water mixture, and castor oil were used. Capillaries of inside diameter 0·085–0·27 cm fabricated from stainless steel hypodermic tubing were used. In table 1 are listed the physical properties of the liquids, which varied slightly from experiment to experiment because of changes in room temperature and the conditions, needle diameter and average ejection velocity, for which data were taken. The physical properties were measured by standard means and found to be in agreement with literature or catalogue values. The table also lists the symbols used in the accompanying figures.

For a given liquid and capillary there was a lower limit on the velocity for which good data could be obtained There were two reasons for this. In some cases the jet was affected by gravity before rearrangement was complete, and in other cases the liquid wetted the edge of the needle giving an initial diameter larger than the inside diameter of the capillary. Runs where either of these two effects occurred were rejected. On the other hand, at sufficiently high ejection velocities a third limitation on the data was encountered: the viscous dissipation in the needle was so large that the viscosity was non-uniform and the velocity profile was significantly altered from the parabolic. Since this effect is accompanied by a flatter initial velocity profile, it was made manifest by χ being closer to unity than one would have expected. We have restricted our data to runs for which the maximum point temperature rise was less than 5 °C as calculated from the theory of Brinkman (1951) for the viscous heating of a fluid (of constant viscosity) flowing in a tube of constant wall temperature. Thus, for castor oil flowing in a tube of diameter 0·22 cm we are limited by viscous heating to the Reynolds numbers less than 24, and by gravitational acceleration to the Reynolds numbers greater than 4.

Jet shapes were measured from flash photographs taken with a 5×7 in. camera using a 25 mm lens. The light from a microflash unit of $0{\cdot}5\,\mu$sec duration was directed onto a ground-glass plate behind the jet so that a shadow photograph was obtained. In each photograph, along with the jet, there appeared a wire of known diameter, so that absolute lengths could be computed (although only ratios were required). The photographs were taken at a magnification of about 10:1 and were read on a travelling microscope. The measured jet diameters are probably accurate to more than three significant figures.

Liquid	Capillary diameter (cm)	Range of the initial Reynolds number $2a_0\overline{w}_0/\nu$	Average value of the surface-tension parameter $\rho\sigma a_\infty/\mu^2$	Corresponding symbol used on figures
White oil	0·084	30–102	2·9	□
μ = 0·64 to 0·69 poise	0·181	22–195	6·3	■
ρ = 0·88 g/cm^3	0·240	46–124	8·3	⊟
σ = 30 dyne/cm	0·269	49–200	9·4	⊞
Glycerol–water mixture	0·120	3–26	0·20	○
μ = 4·6 to 5·2 poise	0·181	4–62	0·30	●
ρ = 1·25 g/cm^3	0·269	4–37	0·45	⊕
σ = 63 dyne/cm	—	—	—	
Castor oil				
μ = 8·4 to 9·0 poise	0·216	4–24	0·054	▲
ρ = 0·96 g/cm^3	—	—	—	
σ = 34 dyne/cm	—	—	—	

Table 1. Experimental conditions

4. Experimental results

In figure 2 is shown a series of jet shapes for the flow of the glycerol–water mixture at the different Reynolds numbers leaving the 0·181 cm diameter needle. These runs all have a constant value of about 0·3 for the surface-tension group. For the Reynolds numbers below about 12 the jet diameter increases monotonically with axial distance, but the magnitude of the increase diminishes as the Reynolds number is raised. Above a Reynolds number of approximately 17 the jet diameter monotonically decreases with axial distance and the magnitude of the change increases as the Reynolds number increases. Between the Reynolds numbers 12 and 17 the jet diameter first decreases and then increases as the axial distance is increased. Because of their close correspondence, it is tempting to associate the Reynolds number for which the minimum of the jet shape first sets in with the Reynolds of the asymptotic line $Re = 4\pi$, and the Reynolds number where the minimum disappears with the bifurcation point at $Re_\infty = 16{\cdot}8$. The Reynolds number for which the final diameter is the same as the initial jet diameter is approximately 14·4.

Figure 3 is a plot of the ratio of the final diameter to the initial diameter as a function of the Reynolds number. Although the value of the surface-tension

group S varied from 0·054 to 9·4, the data were all represented by a single curve (once the runs where there was significant heating were eliminated). Middleman & Gavis inferred from their data that, as the Reynolds number approached zero, χ approached a constant value and as Re tended towards infinity it approached

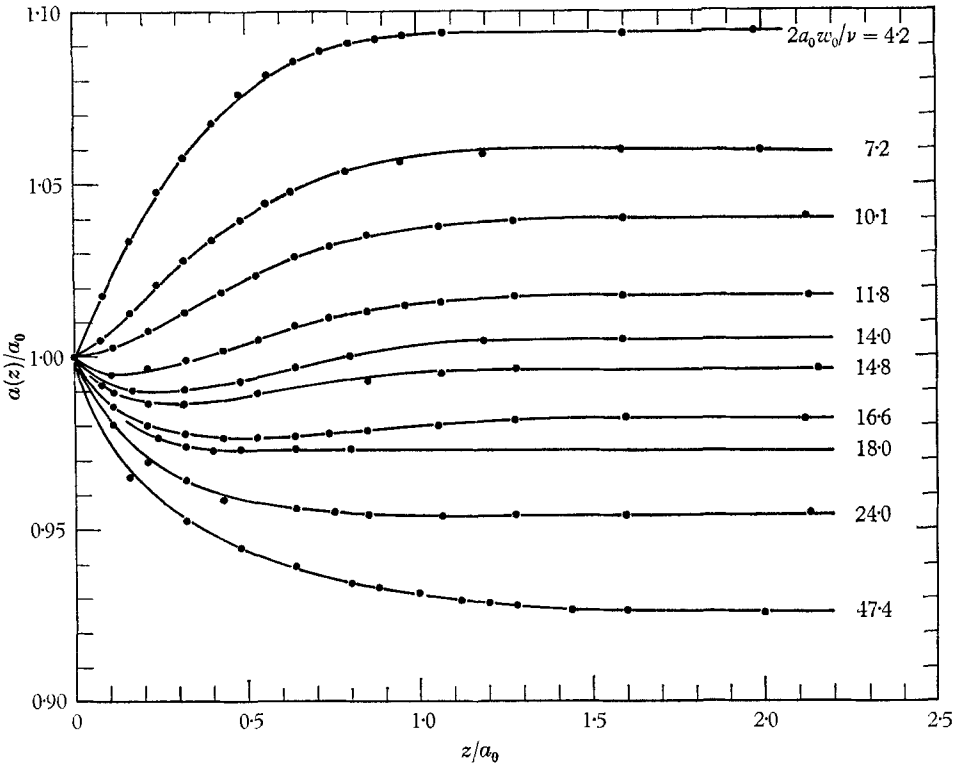

FIGURE 2. Jet shapes for a series of the Reynolds numbers. The surface tension parameter is roughly constant at 0·3.

a second value, namely Harmon's result, $\chi = \frac{1}{2}\sqrt{3}$. At our highest Reynolds numbers, between 100 to 200, the value of χ was roughly constant at 0·885. This value is significantly larger than Harmon's expectation. The difference can most likely be attributed to a combination of viscous heating in the needle and air friction on the jet, both of which would tend to increase χ for contracting jets. At the other extreme, our data for the Reynolds number as low as 4 (where $\chi = 1{\cdot}10$) show no sign of approaching a constant expansion (at least when presented on a linear plot as in figure 3).

In order to test the perturbation theory, the data from each run were plotted in the form $\log|a-a_\infty|/a_\infty$ *vs.* z/a_∞. Except for the points for axial distances less than one-half radius and the points for large axial distances (after about two to three radii), where there was large experimental error in determining the difference $(a-a_\infty)$, the data gave straight lines indicating exponential decay. A few typical plots are shown in figure 4. The curves shown are for the glycerol–water mixture issuing from the 0·120 cm diameter capillary. From the slope of such plots the damping coefficient was determined. The damping coefficient is

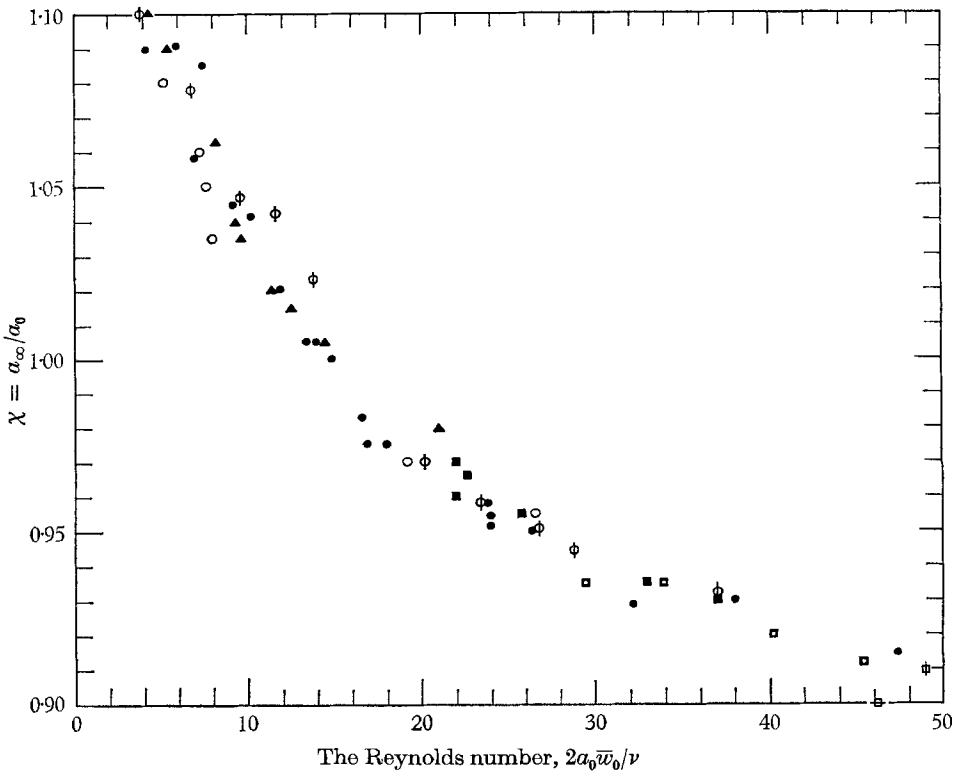

FIGURE 3. Ratio of the final jet diameter to the initial jet diameter as a function of the Reynolds number. For the meaning of the symbols see table 1.

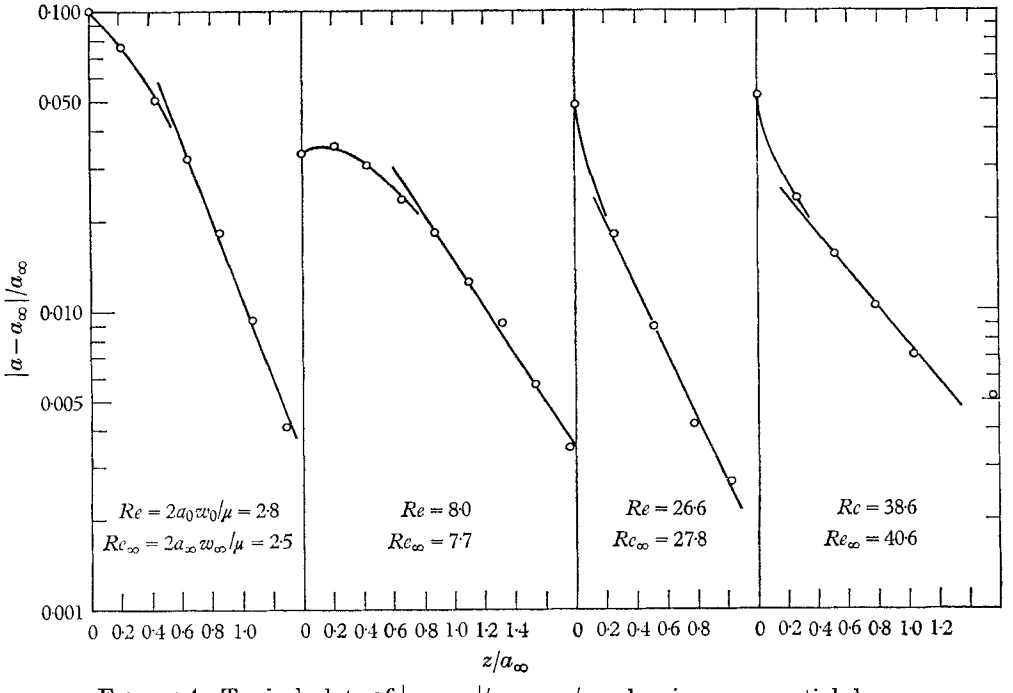

FIGURE 4. Typical plots of $|a-a_\infty|/a_\infty$ *vs.* z/a_∞ showing exponential decay.

presented as a function of the final Reynolds number in figure 5. The most striking feature of the correlation is the apparent discontinuity in γ at a final Reynolds number somewhere between 16 and 20. Because of the very slight changes in jet radius in this region it is difficult to identify the exact point of discontinuity, but it is interesting to note that it does occur within the Reynolds number range where the theoretical eigenvalue exhibits its peculiar behaviour,

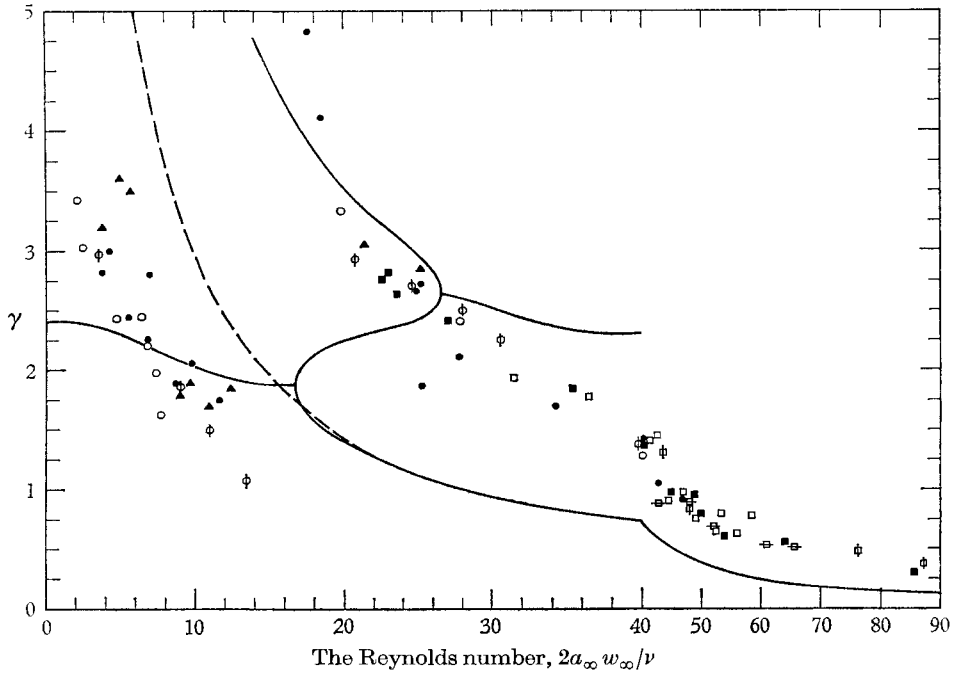

FIGURE 5. Damping coefficient as a function of the final Reynolds number. For the meaning of the symbols see table 1. ———, Perturbation theory for $S = 0$; – – – –, Bohr's theory.

when the surface-tension parameter is between 0 and 10. Again, there seems to be no significant variation of the damping coefficient with the surface-tension parameter for the range of variables studied here. Also shown in the drawing are the predictions of the perturbation theory presented above for $S = 0$, and Bohr's prediction.

The data are in qualitative agreement with the theory advanced here. For example, in the final Reynolds-number range, where the theoretical eigenvalue is multi-valued, the experimental damping coefficient shows a discontinuity. For the final Reynolds numbers less than about 14, where the eigenvalue is complex, the experimental value is in order-of-magnitude agreement with the real part of the calculated eigenvalue. Incidentally, when the eigenvalue is complex one would expect that the jet surface as a function of axial distance would exhibit a damped oscillation. Although the existence of a minimum jet diameter might be taken as some evidence of this, it should be pointed out that the calculation showed that the real part of the complex eigenvalue was always sufficiently larger than the complex part for the jet to decay to its (experi-

mentally) final diameter well within the distance of one wavelength. For the final Reynolds numbers above 20, the damping coefficient is a monotonic decreasing function of the Reynolds number, and for the final Reynolds numbers above 40, the shape of the curve is in agreement with the predicted shape.

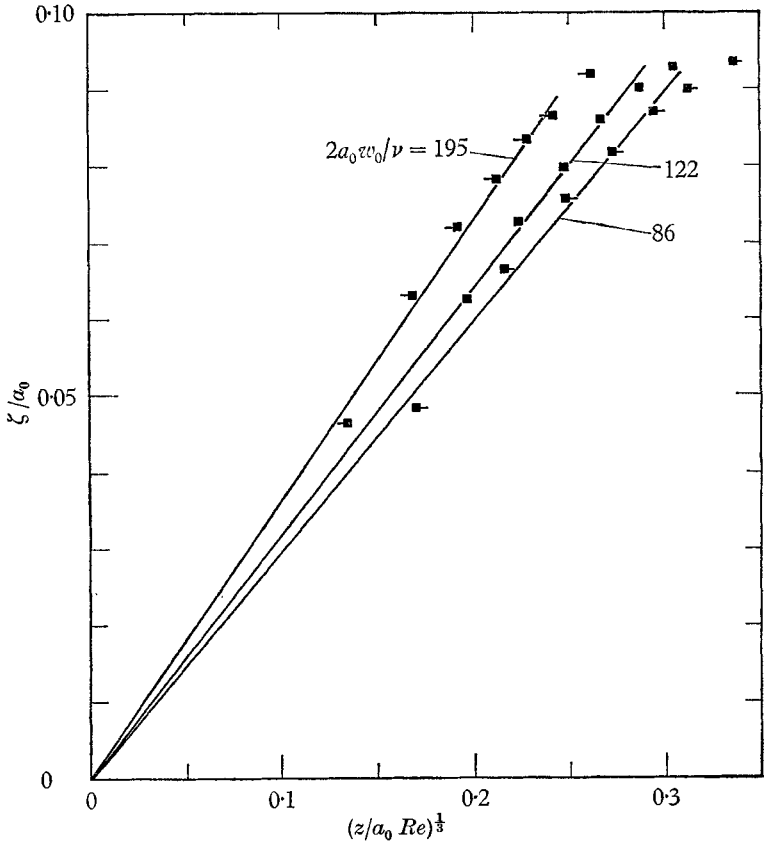

FIGURE 6. Typical plots of $(a_0-a)/a$ *vs.* $(z/a_0 Re)^{\frac{1}{3}}$ to test the boundary-layer analysis.

The experimental values are, however, larger by about a factor of 2. In view of the fairly rapid decay of the jet shape—the change is complete in one to two jet diameters—it is possible that using only the term involving the lowest eigenvalue is not sufficient to represent this region of rapid decay in which the data were taken. If higher eigenvalues are important, then the experimental damping coefficient would lie above the predicted values for the lowest eigenvalue. To take into account higher terms would require evaluation of the constants, A_n, in the series expression $a = a_\infty + \Sigma A_n e^{-\gamma_n z/a_\infty}$. These cannot be evaluated without first establishing the orthogonality of the stream functions and determining the weighting functions. Even so, because of the approximations made, one should not expect the predictions to hold near the needle exit.

Another way of displaying the apparent discontinuity in the experimental data is to plot, as suggested by Middleman (1964), the number of diameters down-

stream required to bring the jet to within 1 % of its final diameter. Middleman presented data for the Reynolds numbers below 10 and above 100 and drew a straight line through the points on a log-log plot. Our data, however, show a very marked decrease in this required length for the Reynolds numbers between 17 and 40. There appear to be two separate curves which lie on either side of Bohr's line as shown in Middleman's figure 2, our data falling on one curve for the Reynolds numbers less than 14 and on the other for the Reynolds numbers greater than 17. The Reynolds number for which this abrupt change in required length occurs is thus seen to be roughly the same as that for the abrupt change in damping coefficient.

The boundary-layer approach near the needle exit predicts that the decrease in jet radius should vary as the cube root of the axial distance downstream. In figure 6 we plot $(a_0-a)/a_0$ *vs.* $(z/a_0Re)^{\frac{1}{3}}$ for several of the runs having the largest Reynolds number. For $(z/a_0Re)^{\frac{1}{3}}$ less than about 0·25 the plots are straight lines through the origin, but as the axial distance increases above this value the plots level off, indicating the finite total change in jet diameter ($\chi \approx \frac{1}{2}\sqrt{3}$). The slope of the linear portion increases slightly as the Reynolds number increases, but is always significantly less than the predicted slope of 0·703. The runs shown are for white oil issuing from a 0·181 cm diameter capillary. For $2\bar{w}_0 a/\nu = 86$, 122, and 195, the values of the slope were 0·30, 0·32, and 0·37, respectively. The discrepancy between these and the predicted slope of 0·703 may be due to the smallness of the Reynolds number, but more likely it is due to the interaction of the peripheral boundary layer with the core fluid.

5. Summary

The shape of a jet of Newtonian liquid issuing from a capillary needle into air has been studied theoretically and experimentally. One theoretical approach, a perturbation analysis about the final state of the jet, predicts that the jet radius will decay exponentially to its final value and gives the damping coefficient (i.e. the lowest eigenvalue) as a function of the final Reynolds number, $2a_\infty w_\infty/\nu$, and a surface tension parameter, $S = \rho\sigma a_\infty/\mu^2$. For non-infinite values of the surface-tension parameter the theoretical damping coefficient exhibits peculiar behaviour when the final Reynolds number is less than about 27, becoming multi-valued or complex. This peculiarity is reflected in the experimental damping coefficient by the occurrence of a discontinuity in the same Reynolds'-number range. Otherwise the experimental and theoretical damping coefficients are in agreement as to dependence on the Reynolds number, but the experimental values are larger by a factor of 2. A boundary-layer approach was developed which predicts that for short axial distances and the large Reynolds numbers the change in jet radius varies as the cube root of the axial distance. This cube-root dependence is confirmed, but the observed coefficient is less by a factor of 2 than the predicted one.

The most likely reason for the discrepancy between the perturbation analysis and the measurements is that the decay is so rapid that more than just the lowest eigenvalue term is required to represent the data. The discrepancy between the

boundary-layer analysis and the measurements may be due to the interaction of the peripheral boundary layer with the core of the jet, which interaction was neglected in the theory, or to the smallness of the Reynolds numbers. Once reliable estimates of the jet shapes for large and small axial distances are at hand, a matching procedure might be developed to predict the entire jet shape.

The present work suggests several experiments which would be of value. To test the boundary-layer analysis it would be of interest to measure the shapes of jets with the much higher Reynolds numbers (on the order of 1000 to 2000). Data for jets with large values of the surface-tension parameter ($S > 100$) would be of interest in view of the large difference in the theoretical curves for large and small values of S at the low Reynolds numbers. Also, the complication introduced by viscous heating within the needle deserves investigation because of the use of capillary jets to obtain rheological data for very viscous non-Newtonian liquids.

REFERENCES

BRINKMAN, H. C. 1951 Heat effects in capillary flow I. *Appl. Sci. Res.* A, **2**, 120.

BOHR, N. 1909 Determination of the surface tension of water by the method of jet-vibration. *Phil. Trans.* A, **209**, 281.

GAVIS, J. 1964 Contribution of surface tension to expansion and contraction of capillary jets. *Phys. Fluids*, **7**, 1097.

GOLDSTEIN, S. 1930 Concerning some solutions of the boundary layer equations of hydrodynamics. *Proc. Camb. Phil. Soc.* **26**, 1.

HARMON, D. B. 1955 Drop sizes from low speed jets. *J. Franklin Inst.* **259**, 519.

MEKSYN, D. 1961 *New Methods in Laminar Boundary-Layer Theory.* Oxford: Pergamon Press.

MIDDLEMAN, S. & GAVIS, J. 1961 Expansion and contraction of capillary jets of Newtonian liquids. *Phys. Fluids*, **4**, 355. Errata: *Phys. Fluids*, **4**, 1450.

MIDDLEMAN, S. 1964 Profile relaxation in Newtonian jets. *Ind. Eng. Chem. Fundamentals*, **3**, 118.

SCRIVEN, L. E. & PIGFORD, R. L. 1959 Fluid dynamics and diffusion calculations for laminary liquid jets. *A.I.Ch.E. J.* **5**, 397.